

# A threshold-based earthquake early warning using dense accelerometer networks

Aldo Zollo,<sup>1</sup> Ortensia Amoroso,<sup>1</sup> Maria Lancieri,<sup>1,2</sup> Yih-Min Wu<sup>3</sup> and Hiroo Kanamori<sup>4</sup>

<sup>1</sup>Department of Physics (RISSC-Lab), University of Naples 'Federico II', Italy. E-mail: aldo.zollo@unina.it

<sup>2</sup>Ecole Normale Supérieure, Paris, France

<sup>3</sup>Department of Geosciences, National Taiwan University, Taipei, Taiwan

<sup>4</sup>Seismological Laboratory, California Institute of Technology, Pasadena, CA, USA

Accepted 2010 August 4. Received 2010 July 24; in original form 2010 April 30

## SUMMARY

Most earthquake early warning systems (EWS) developed so far are conceived as either 'regional' (network-based) or 'on-site' (stand-alone) systems. The recent implementation of nationwide, high dynamic range, dense accelerometer arrays makes now available, potentially in real time, unsaturated waveforms of moderate-to-large magnitude earthquakes recorded at very short epicentral distances (<10–20 km). This would allow for a drastic increase of the early warning lead-time, for example, the time between the alert notification and the arrival time of potentially destructive waves at a given target site. By analysing strong motion data from modern accelerograph networks in Japan, Taiwan and Italy, we propose an integrated regional/on-site early warning method, which can be used in the very first seconds after a moderate-to-large earthquake to map the most probable damaged zones. The method is based on the real-time measurement of the period ( $\tau_c$ ) and peak displacement (Pd) parameters at stations located at increasing distances from the earthquake epicentre. The recorded values of early warning parameters are compared to threshold values, which are set for a minimum magnitude 6 and instrumental intensity VII, according to the empirical regression analyses of strong motion data. At each recording site the alert level is assigned based on a decisional table with four alert levels defined upon critical values of the parameters Pd and  $\tau_c$ , which are set according to the error bounds estimated on the derived prediction equations. Given a real time, evolutionary estimation of earthquake location from first *P* arrivals, the method furnishes an estimation of the extent of potential damage zone as inferred from continuously updated averages of the period parameter and from mapping of the alert levels determined at the near-source accelerometer stations. The off-line application of the method to strong motion records of the *M<sub>w</sub>* 6.3, 2009 Central Italy earthquake shows a very consistent match between the rapidly predicted (within a few seconds from the first recorded *P* wave) and observed damage zone, the latter being mapped from detailed macroseismic surveys a few days after the event. The proposed approach is suitable for Italy, where, during the last two decades, a dense network of wide dynamic-range accelerometer arrays has been deployed by the Department of Civil Protection (DPC), the Istituto Nazionale di Geofisica e Vulcanologia (INGV) and other regional research agencies.

**Keywords:** Earthquake ground motions; Earthquake source observations; Early warning

## 1 INTRODUCTION

In the past two decades, progresses have been made towards implementation of earthquake early warning systems (EWS) in many active seismic regions of the world.

In particular, operational EWS are actually running in Japan (Nakamura 1984; Nakamura 1988; Odaka *et al.* 2003; Horiuchi *et al.* 2005), Taiwan (Wu & Teng 2002; Wu & Zhao 2006) and Mexico (Espinosa-Aranda *et al.* 2009), whereas other systems are under testing or development in California (Allen & Kanamori

2003; Allen *et al.* 2009a,b, Böse *et al.* 2009), southern Italy (Zollo *et al.* 2006; Zollo *et al.* 2009a,b), Turkey (Alcik *et al.* 2009) and Romania (Böse *et al.* 2007).

EWS are aimed at providing a rapid notification of the potential damaging effects of an impending earthquake, through fast telemetry and processing of data from dense instrument arrays deployed in the source region of the event of concern or in the area surrounding the target infrastructure (Kanamori 2005).

Most developed EWS are conceived as either 'regional' (network-based) or 'on-site' (stand-alone) systems (Kanamori

2005). A ‘regional’ EEWS is based on a dense sensor network covering a portion or the entirety of an area that is threatened by earthquakes. The relevant source parameters (event location and magnitude) are estimated from the early portion of recorded signals and are used to predict, with a quantified confidence, a ground motion intensity measure at a distant site where a target structure of interest is located. An ‘on-site’ EEWS consists of a single sensor or an array of sensors deployed in the proximity of the target structure that is to be alerted, and the peak amplitude and/or predominant period on the initial *P*-wave motion are used to predict the ensuing peak ground motion (mainly related to the arrival of *S* and surface waves) at the same site.

An optimal performing EEWS can be defined as the system providing at the same time the largest ‘lead-time’ (e.g. the time interval between the arrival of the damaging waves and alert notification) and minimum prediction error on peak ground motion (e.g. difference between observed and predicted logarithmic peak motion amplitude) (Zollo *et al.* 2009a,b).

The main advantage of a network-based EEWS is that a continuously updated and more accurate estimation of source parameters (location and magnitude) is available in real time, as new data are acquired by the network. The accuracy on peak ground motion prediction at distant sites is essentially related to the parameter uncertainty of the used ground motion prediction equation (GMPE). On the other hand, for an on-site EEWS, the alert on an impending earthquake damage at the target site is mainly issued based on a local measurement of *P*-wave ground motion, with no need for accurate estimation of source parameters. In terms of lead-time, a network-based system can provide with a potential warning time a factor of about two longer than for a site-specific, as it can be estimated by theoretical calculations of *P*- and *S*-wave travel times at stations located in the source region and far away, using a standard crustal velocity model.

Wu & Kanamori (2005, 2008) have proposed a methodology for on-site early warning applications aimed at the rapid assessment of earthquake damage potential, which is based on the near source (epicentral distance smaller than 30 km), real-time measurement of the peak displacement (Pd) and predominant period ( $\tau_c$ ) from early *P*-wave signals. The settings of specific thresholds for Pd and  $\tau_c$  allow the system to rapidly issue an earthquake alert based on a four-entry decision-table scheme.

In this note we explore the feasibility of applying a similar approach in Italy, based on the analysis of the strong motion records from the European Strong Motion Data Base and from the larger events ( $M_I \geq 3.9$ ) of the recent 2009, *Mw* 6.3 Central Italy (L’Aquila) earthquake sequence. By extending the observation epicentral distance to 100 km, and by comparing data from different worldwide seismic regions, we generalize the Wu & Kanamori (2005) method and propose an integrated regional/on-site early warning method which can be used in the very first seconds after a moderate-to-large earthquake for mapping the most probable damaged zones. The proposed approach is suitable for Italy, where, during the last two decades, a dense network of wide dynamic range accelerometer arrays has been deployed by the Department of Civil Protection (DPC), the Istituto Nazionale di Geofisica e Vulcanologia (INGV) and other regional research agencies.

## 2 DATA PROCESSING AND ANALYSIS

For this study we have analysed 3552 strong motion records from 296 events, which have been recorded in Japan (K-Net), Taiwan

(TSMIP Central Weather Bureau network) and Central Italy (RAN, Department Civil Protection). These records were obtained by the modern digital accelerometer networks operating for about one decade in those countries. The data set includes the acceleration records of the main shock and 12 largest magnitude ( $M_I \geq 3.9$ ) aftershocks of the *Mw* 6.3, Central Italy (L’Aquila) earthquake sequence, which occurred in 2009 April. The distribution of the analysed waveform records as a function of the epicentral distance and magnitude is displayed in Fig. 1. The spanned magnitude range is 4–8.5 with a maximum epicentral distance of 150 km, whereas most of records are acquired at less than 60 km hypocentral distance. The analysed events are for the most occurring at crustal depths ( $z < 50$  km), encompassing different geological and tectonic regions and are associated with various types of faulting mechanisms.

The procedure of data analysis involved sensitivity correction, *P*-phase identification and picking, single and double integration to obtain the velocity and displacement records, and causal Butterworth filtering with a high pass frequency of 0.075 Hz. The choice of the filter was made by trial and error to remove long-period artificial fluctuations contaminating the records with a relatively low signal-to-noise ratio.

The first *P*-wave arrival is picked on the unfiltered vertical acceleration components, and the peak displacement Pd (Wu & Kanamori 2005; Zollo *et al.* 2006) and the period parameter  $\tau_c$  (Nakamura 1988; Kanamori 2005) (see next section) are measured from the bandpass-filtered displacement and velocity records over a 3-s time window after the first *P* time. To minimize the effect of *S* arrival in the *P*-wave time window, the *P* peak displacement and period parameter have been measured on the high-pass filtered, vertical component of ground motion, assuming that the direct *P* rays are nearly vertical incident to the receiver, due to the generally observed increase of seismic velocities as a function of depth within the Earth.

The peak ground velocity (PGV) is measured from the maximum amplitude on the unfiltered horizontal components of the ground-motion velocity records.

For both Japanese and Italian waveforms data from low magnitude ( $M < 5$ ) events, we had a large scatter of  $\tau_c$  data, the measurement of which is critically dependent on the signal-to-noise ratio in the selected *P* wave window. The data scatter can be reduced by selecting for the analysis only those data for which the peak *P* velocity (*PV*max) over the selected time window is larger than a given threshold, 0.05 cm s<sup>-1</sup>. This threshold was set after several trials on Japanese and Italian waveform data.

Another signal artefact appeared from visual inspection of some acceleration and velocity waveforms from the Japanese K-Net. Some traces showed a sudden step on the acceleration trace, which seems to happen when very high-frequency energy arrives. This is most likely originated from the sensor spring system and/or electronics. We have decided to remove these records from our analyses. As the sensors of the K-Net were replaced by new types of sensors, this problem seems to have been almost eliminated.

In Fig. 2 is shown an example of waveform data from two stations which recorded the *Mw* 6.3, 2009 earthquake in L’Aquila (central Italy).

## 3 EMPIRICAL PREDICTION EQUATIONS FOR A THRESHOLD-BASED EARLY WARNING SYSTEM

The early warning procedure that we propose is based on the real time, simultaneous measurements of peak displacement (Pd) and

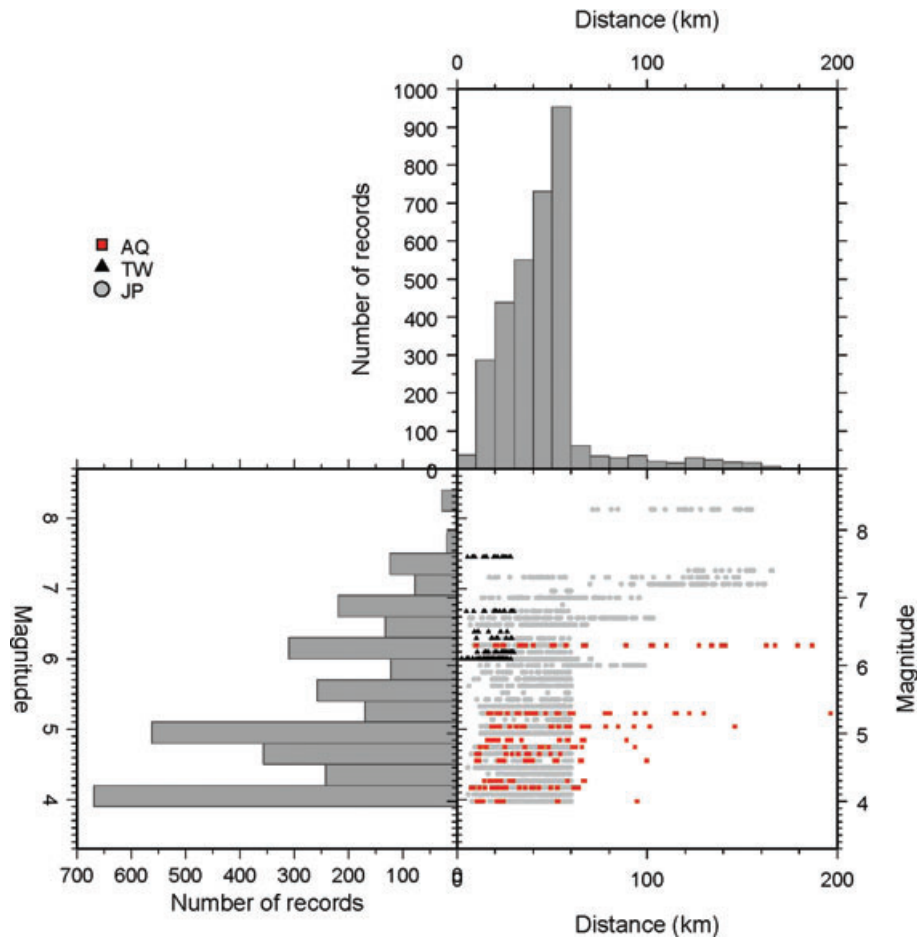


**Figure 1.** Distribution of the number of earthquake records as a function of the magnitude and epicentral distance. Waveform data are extracted from the Japan, Taiwan and Italy (Aquila 2009 earthquake sequence) databases.

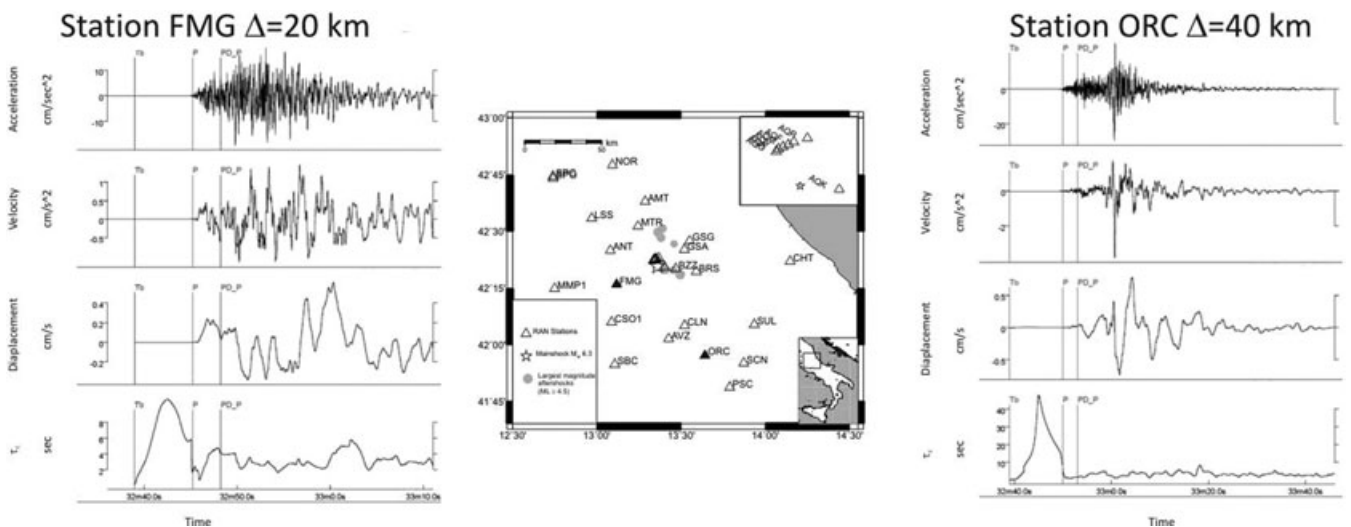


**Figure 2.** Examples of waveform data from the  $M_w$  6.3, 2009 L'Aquila main shock recorded at stations FMG and ORC of the RAN-DPC network in Central Italy. The acceleration, velocity displacement and  $\tau_c$  time-series are plotted from top to the bottom. The selected time window for Pd and  $\tau_c$  measurements is delimited by vertical bars. The  $\tau_c$  trace is computed as the continuous measurement of the period parameter in consecutive 3-s wide windows, and each value corresponds to the one measured in the preceding 3-s time window. The map shows the location of RAN accelerometric stations and main- and aftershocks earthquakes whose data are used for the analysis in this study.

the period parameter  $\tau_c$  for a 3-s window after the first  $P$ -arrival time at an array of accelerometer stations located at increasing distances from the epicentre. Based on the off-line analysis of strong motion records from Japan, Taiwan and Italy we determine three ground-motion empirical relationships (PGV versus Pd,  $\tau_c$  versus magnitude and Pd versus  $\tau_c$  and distance) which can be used in real time to rapidly predict the potential for earthquake damage near the recording site and estimate the approximate extent of the potential damage zone (PDZ).

### 3.1 PGV versus Pd

To rapidly assess the potential for earthquake damage, Wu & Kanamori (2005) suggested the use of Pd as a proxy for PGV, based on the observed correlation between the early  $P$ -wave peak displacement and strong ground-motion parameters.

From the comparison with observed intensity maps, Wald *et al.* (1999), observed that peak velocity and earthquake damages are correlated through the intensity parameter  $I_{MM}$  (Modified Mercalli Intensity) for intensities larger than VII.  $I_{MM}$  is an instrumentally derived, estimated Modified Mercalli Intensity parameter, relating the recorded ground motions to the expected felt and damage distribution. The instrumental intensity map is based on a combined regression of recorded peak acceleration and velocity amplitudes. The relationship between PGV and  $I_{MM}$  is implemented by the USGS in the ShakeMap generation procedure for rapid estimation of strong ground shaking after a damaging earthquake. Thus, the potential damaging effects of a moderate-to-large earthquake can be rapidly predicted by Pd measurements using the correlation of this parameter with peak motion velocity.

In Fig. 3 the PGV data measured from the integrated acceleration records in Japan, Taiwan and Italy (2009  $M_w$  6.3 L'Aquila main shock and aftershocks) are plotted as a function of peak displacement measured over a 3-s window after the first  $P$  arrival on the vertical component of double-integrated acceleration records. For the Taiwan data sets, records analysed by Wu & Kanamori (2005) have been considered for this analysis (with a maximum epicentral

distance of 30 km) whereas a larger maximum distance (60 km) has been considered for data from Japan and L'Aquila sequence data sets. Overall the log (PGV) appears linearly correlated with log (Pd) over about four orders of magnitude independently of the maximum distance and earthquake size within the considered ranges. The data distribution that are obtained by selecting a maximum epicentral distance of 30 km and 60 km are shown in Figs 3(a) and (b), respectively. No significant changes are noted in the parameters of the log (PGV) versus log (Pd) relationship by increasing the epicentral distance, except a slight increase of the standard error. The empirical relationship retrieved for the 60-km data set has been used for further analyses.

In particular, the L'Aquila earthquake data show a pattern of parameter variability consistent with that from other regions, suggesting that the PGV versus Pd correlation is independent also of the tectonic environments and specific source and propagation effects like directivity, radiation pattern, anelastic attenuation and site effects. We note the relatively high values of Pd and PGV greater than 1 cm and 30 cm s<sup>-1</sup> recorded during the  $M_w$  6.3 L'Aquila main shock at stations less than 10 km from the epicentre.

Considering a maximum recorded distance of 60 km, we obtain a regression relation

$$\log(\text{PGV}) = 0.73 (\pm 0.01) \log(\text{Pd}) + 1.30 (\pm 0.02), \quad (1)$$

where PGV is in cm s<sup>-1</sup> and Pd is in centimetres.

### 3.2 $\tau_c$ versus $M$

Nakamura (1988) first proposed the measurement of the predominant period ( $\tau_{\max}^p$ ) from the first  $P$  wave train to be used for early warning purposes. The method has been extensively applied to broad-band and strong-motion records from several seismic regions worldwide, showing that  $\tau_{\max}^p$  scales with earthquake magnitude while being not dependent on the epicentral distance up to a few hundred kilometres of the event (Allen & Kanamori 2003; Allen *et al.* 2009a,b). Alternatively, Wu & Kanamori (2005) adopted a different approach based on the estimation of the period

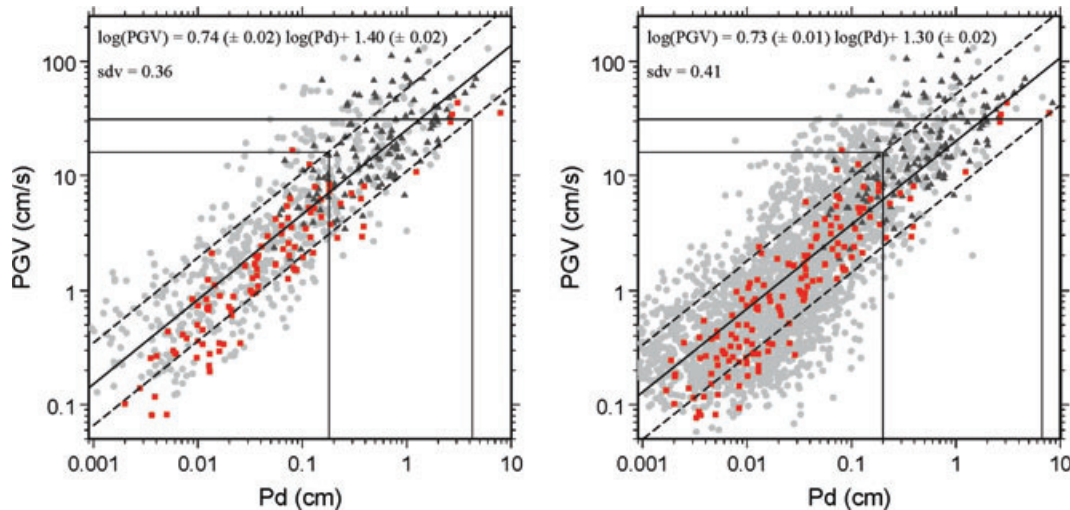


**Figure 3.** Plot of peak ground velocity (PGV) versus initial peak displacement (Pd), for records at epicentral distances smaller than 30 km (left-hand panel) and 60 km (right-hand panel). The figures display data from Japan (grey dots), Taiwan (black triangles) and Central Italy (red squares) earthquakes. Pd is measured (in centimetres) over a 3-s window after the first  $P$  arrival on bandpass-filtered vertical displacement records. PGV is the max of the two horizontal velocity records (in cm s<sup>-1</sup>). The relationship between PGV and instrumental intensity ( $I_{MM}$ ) (Wald *et al.*, 1999) is used to estimate the bounds (horizontal and vertical solid lines) for Pd and PGV associated to an instrumental intensity  $I_{MM} = VII$ ; sdv indicates the standard error for the best-fit regression equations, also reported in the figures.

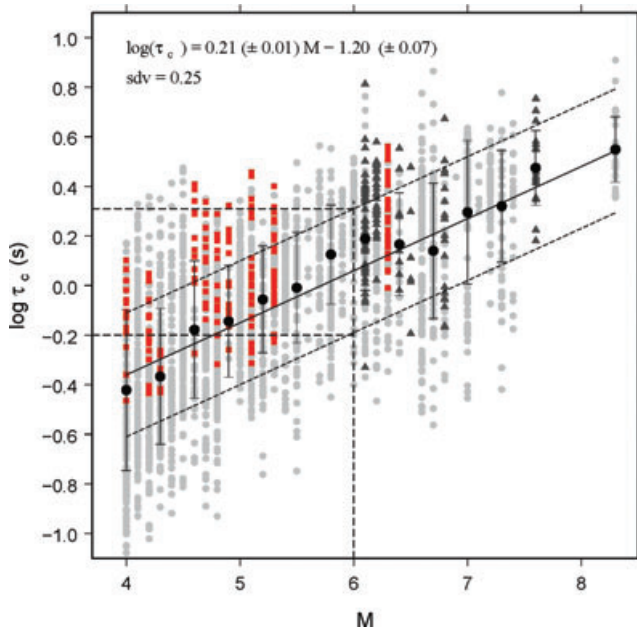


**Figure 4.** Plot of the period parameter  $\tau_c$  versus magnitude. The figure displays data from Japan (grey dots), Taiwan (black triangles) and Central Italy (red squares) earthquakes. The best-fit line and the associated standard error bounds are computed on average binned data ( $\Delta M = 0.3$ ) (black dots), weighted by the standard deviation (vertical error bars). The misfit standard error bounds (dashed lines) allow to define the expected 1- $\sigma$  variation of  $\log(\tau_c)$  for a threshold magnitude of 6 (dashed lines).

parameter ( $\tau_c$ ).

$$\tau_c = 2\pi \sqrt{\frac{\int_0^{\tau_o} u^2(t) dt}{\int_0^{\tau_o} v^2(t) dt}}, \quad (2)$$

where  $u$  and  $v$  are displacement and velocity, respectively. The integrals in (2) are computed over a time window  $(0, \tau_o)$  starting from the first  $P$  arrival and  $\tau_o$  is generally set at 3 s.

$\tau_c$  can be considered as the average period of the  $P$ -wave signal and it has the main advantage that the period estimation in real time is performed on the actual  $P$ -wave window, being less influenced than  $\tau_{\max}^p$  by the filter parameters and pre-event noise (Shieh *et al.* 2008). Shieh *et al.* (2008) suggest that the joint measurement and average of  $\tau_c$  and  $\tau_{\max}^p$  values contribute to a net reduction of the uncertainty in magnitude estimation.

For the purpose of this work we have estimated  $\tau_c$  from the vertical component of strong motion records of Taiwan, Japan and the 2009 L'Aquila earthquakes to investigate and determine the relationship of the period parameter with magnitude in the whole analysed magnitude range  $4 < M < 8.3$  (Fig. 4). The best-fit regression line has been computed on average binned data ( $\Delta M = 3$ ) weighted by the standard deviation for data in each bin.

$$\log(\tau_c) = 0.21(\pm 0.01)M - 1.19(\pm 0.08), \quad (3)$$

where  $\tau_c$  is measured in seconds and  $M$  is the moment magnitude. The standard error bounds allow us to define the expected 1- $\sigma$  variation of  $\log(\tau_c)$  for a magnitude  $M$  6, which is considered as a threshold magnitude value for early warning in this study.

### 3.3 Pd versus $\tau_c$ and distance

With the aim to infer a rapid estimation of the extent of the PDZ (see next section), we have determined the empirical relationship

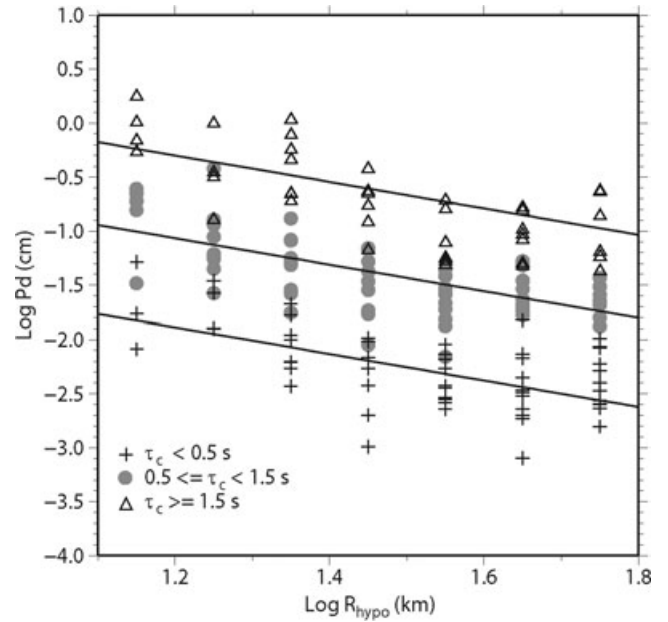


**Figure 5.** Plot of the peak displacement  $Pd$  as a function of the period parameter and hypocentral distance  $R_{\text{hypo}}$ . The original data from the three considered regions have been merged and binned in cells of constant size over the sampled distance and period space  $[0.1 \log(R_{\text{hypo}}) \times 0.05 \log(\tau_c)]$ . Binned data are plotted with different symbols depending on the considered range of variation for parameter  $\tau_c$ . The theoretical best-fit lines are plotted from eq. 4 for fixed values (0.3 s, 0.8 s and 2 s) of the parameter  $\tau_c$ .

which relates the initial  $P$  peak ground displacement with the period parameter  $\tau_c$  and hypocentral distance,  $R$ . Given the observed dependency of the period parameter with magnitude this relationship is similar to a GMPE for the parameter  $Pd$  in the investigated range of distances. A multivariate linear regression analysis has been performed to search the best-fit parameters of the equation

$$\log(Pd) = A + B \log(\tau_c) + C \log(R), \quad (4)$$

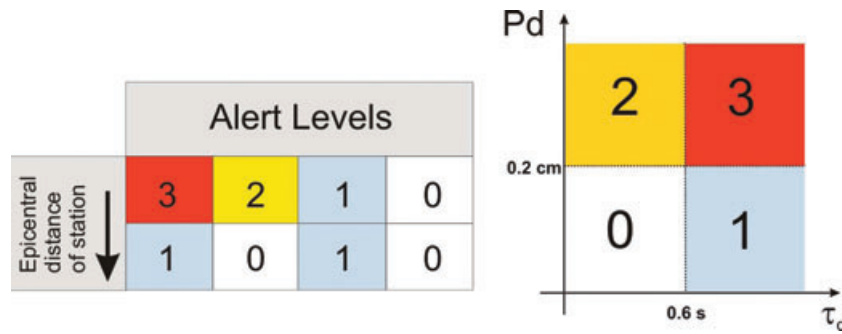
where  $R$  is the hypocentral distance. To estimate the coefficients  $A$ ,  $B$  and  $C$  of eq. 4,  $\tau_c$  and distance data have been initially binned in cells of constant size over the sampled distance and period space. The mean value of the peak displacement parameter and its standard deviation for each cell have been computed and used for the weighted least-square fitting of eq. 4, by assigning a weight to each data point. The weights are inversely proportional to the cell standard deviation of  $Pd$ . The results of the regression analyses provided values of coefficients  $A = 0.6 \pm 0.1$ ,  $B = 1.93 \pm 0.03$  and  $C = -1.23 \pm 0.09$ , with a standard error of 0.70, with  $Pd$  measured in cm,  $\tau_c$  in seconds and  $R$  in km.

Fig. 5 shows the observed  $Pd$  distribution as a function of the distance and period parameter, along with the best-fit GMPEs obtained for different values of  $\tau_c$ .

## 4 ALERT LEVELS AND STRATEGY FOR EARLY WARNING NOTIFICATION

The proposed early warning system is based on the real-time measurement of the parameters  $Pd$  and  $\tau_c$  in a short time window after the first  $P$  wave at a single site of a widely distributed and interconnecting network of strong motion sensors.

A threshold-based alert system requires the definition of alert levels which are set depending on *a priori* selected threshold values for the real time-measured ground-motion parameters. According



**Figure 6.** Alert levels and threshold values for observed early warning parameters. We define four alert levels: 3 = damages expected nearby and far-away from station; 2 = damages expected only nearby the station; 1 = damages expected only far way from the station and 0 = no expected damage. Left: expected variation of alert levels as a function of the epicentral distance. Colours are assigned according to the scheme shown in the right-hand panel. Table reports the allowed transitions from each initial level as a function of the distance from the earthquake epicentre. Right: Pd versus  $\tau_c$  diagram showing the chosen threshold values and the regions delimiting the different alert levels.

to Wu & Kanamori (2005) and using the empirical relationships eqs 1 and 3, we define four alert levels depending on the measured values of the parameters Pd,  $\tau_c$  at a given strong motion site (Fig. 6).

The threshold values for Pd and  $\tau_c$  (0.2 cm and 0.6 s, respectively) have been chosen to have the maximum alert level (level 3) for an earthquake with predicted magnitude  $M \geq 6$  and damage effects in the epicentral area associated with an instrumental intensity  $I_{MM} \geq 7$ . In particular, the peak displacement threshold is set based on the Wald *et al.* (1999) relationships between instrumental intensity and PGV used for ShakeMap computation and the estimated 1- $\sigma$  error bounds on the PGV versus Pd relationship obtained in this study (Fig. 3). The  $\tau_c$  threshold is instead inferred from the 1- $\sigma$  error bounds of the  $\tau_c$  versus  $M$  relationship for an  $M = 6$  (Fig. 4).

It should be noted that if we consider a series of measurements Pd,  $\tau_c$  at sites located at increasing epicentral distances, not all the transitions from one alert level to another are allowed (Fig. 6). This is mainly related to the attenuation of  $P$  peak displacement with distance, for which, beyond a given distance, the parameter Pd is expected to be smaller than the threshold value. The table in Fig. 6 illustrates the possible combination of alert levels as detectable at sites located at increasing distances from the epicentre.

The alert scheme displayed in Fig. 6 can be used to define the early warning notification procedure and strategy, given a dense network of accelerometers deployed in- and outside the epicentral area of a potentially damaging earthquake. As the  $P$  wave front expands away from the epicentre, local measurements of  $\tau_c$  and Pd can be performed at strong motion stations located at increasing epicentral distances, allowing the system to define an alert level for each recording site (Fig. 7). The information about the alert level recorded at near-source stations can be transmitted to more distant sites before the arrival of the  $P$  and of the potentially destructive  $S$  wave train, similar to the procedure used for regional early warning systems. According to the alert scheme in Fig. 6 and depending on the maximum alert level defined at the stations closest to the epicentre, the areal distribution of alert levels provides a fairly accurate estimation of the PDZ, as the area delimiting the maximum alert level sites (two or three) in case of an earthquake occurring within the network.

However, a rough but very rapid estimation of the PDZ extent can also be made from the updated averages of the period parameter  $\tau_c$ , which is recorded at strong motion sites in the near-source region. Fixing the parameter Pd at its threshold value (e.g. 0.2 cm), and using the progressively updated estimations of the period parameter, the

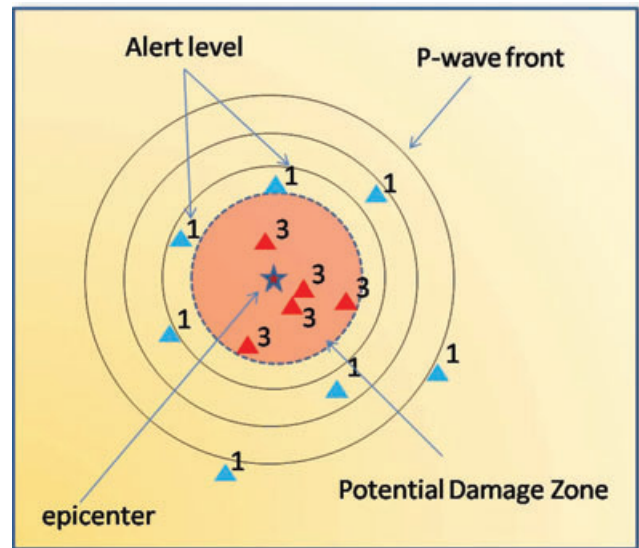


**Figure 7.** Illustration of the early warning procedure. The method foresees a progressive detection of alert levels moving from near- to far-source stations. The local measurements of Pd and  $\tau_c$  allow to define the alert level for that site, define the potential damage/not damaged zone (circular dashed area) an alert to more distant sites and finally make a decision based on both the regional information and the local measurement of ground motion. The extent of the potential damage zone (PDZ) is mapped from the geographical distribution of recorded alert levels and updated averages of  $\tau_c$  as new measurements are available at the network.

Pd GMPE (eq. 4) can be used to determine the radius of the area within which the strong ground motion is expected to produce an instrumental intensity  $I_{MM}$  greater than VII. This information can be available only a few seconds after the recording of the first  $P$  arrival at near-source accelerometers, and it will be confirmed and refined as more measurements of the period parameter are available at more distant stations. In this case an evolutionary, real-time estimate of the earthquake location is needed to map the PDZ. The earthquake location can be obtained from the automatic first  $P$ -picking measurement and a real-time location procedure.

In our application to the  $M_w$  6.3 L'Aquila earthquake records (next section) we have used the methodologies for picking, event binding and location implemented for the southern Italy early warning system PRESTo (Probabilistic and Evolutionary Early Warning System) (Zollo *et al.* 2009a,b; Satriano *et al.* 2010). We used a phase

detector and picker algorithm optimized for real-time seismic monitoring and earthquake early warning; the basic concepts are similar to those of the Baer and Kradolfer picker (Baer & Kradolfer 1987), and the Allen picker (Allen 1978). The real-time location algorithm (RTLloc, Satriano *et al.* 2008) is based on the equal differential time (EDT) formulation (Font *et al.* 2004) and on a fully probabilistic description of the hypocentre. At each time step, the method uses both the arrival times automatically measured at the triggered stations, as well as the implicit information that can be derived from the lack of arrival detections at the other stations, which are not yet reached by the  $P$  waves.

The RTLloc location algorithm is used for the initial estimation of the PDZ extent, through the evaluation of the hypocentral distance by eq. 4. The method is able to provide with a first, approximate epicentral location by using just one station, applying the concept of Voronoi cells (Cua & Heaton 2007; Satriano *et al.* 2008). As far as new  $P$  picks are available, a probabilistic, evolutionary estimation of epicentre, depth and origin time is obtained, with improved accuracy. Tests on synthetic and real data, showed that enough accurate and robust estimation can be obtained using three to four stations depending on the station density and azimuthal coverage of the source (Satriano *et al.* 2010).

## 5 OFF-LINE APPLICATION TO THE $M_w$ 6.3 2009 L'AQUILA EARTHQUAKE IN CENTRAL ITALY

On 2009 April 6 a moderate size earthquake struck the Abruzzo region in Central Italy destroying the entire districts of the town of L'Aquila, and causing several hundred casualties and a series of building collapses in a wide region, mainly south-east of the epicentral area.

The main shock fault plane solution indicates that the earthquake rupture occurred along a NW–SE-oriented normal fault segment, dipping towards the SW, with the city of L'Aquila lying a few kilometres away on the hanging wall (Maercklin *et al.* 2009; Pondrelli *et al.* 2009). Kinematic modelling of strong motion, GPS and in-SAR data suggest a fault length and width of about 20 and 10 km, respectively, with a heterogeneous final slip distribution and rupture velocity on the SW-dipping fault plane (Cirella *et al.* 2009; Yano *et al.* 2009).

Two main aftershocks occurred after the main event with  $M_w$  5.6 and  $M_w$  5.4, respectively activating additional faults at the north-western and south-eastern edges of the main fracture (Falcucci *et al.* 2009) explaining the dense and wide spread aftershock activity (Chiarabba *et al.* 2009).

The main shock was recorded by more than 50 digital accelerometer stations of the Italian Accelerometric Network (RAN) (Fig. 8) owned by the national DPC and located at epicentral distances between 0 and 250 km. Very high values of peak acceleration ( $>0.5$  g) were recorded downtown and nearby the city of L'Aquila (Akinci *et al.* 2010).

A detailed reconstruction of the damage spatial distribution has been performed based on a rapid survey carried out by a joint group of the national DPC and INGV, which provided a map of macroseismic intensity  $I_{MCS}$  (MCS = Mercalli-Cancani-Sieberg Intensity scale) (max  $I_{MCS} = IX-X$ ) (Galli *et al.* 2009).

The Mercalli-Cancani-Sieberg, MCS, is used in Italy as the standard intensity scale that describes the earthquake effects on the built environment. This scale differs from the Mercalli Modified Intensity scale ( $I_{MM}$ ) adopted in other countries and assumed as standard

for ShakeMap computation at USGS (Wald *et al.* 1999). Recently, Faenza & Michelini (2010) derived new regression relationships between  $I_{MCS}$  and peak ground-motion parameters, PGV and PGA, based on the Italian databases of macroseismic information and digital accelerometric waveforms. Combining the empirical relationships retrieved for  $I_{MM}$  versus PGV by Wald *et al.* (1999) and for  $I_{MCS}$  versus PGV by Faenza & Michelini (2010) one obtains  $I_{MCS} = 3.51 + 0.67 I_{MM}$ , so that the threshold value for damage effects of  $I_{MM} = VII$  roughly corresponds to  $I_{MCS} = VIII$ .

In this study, the parameters  $P_d$  and  $\tau_c$  have been measured from a 3-s window after the first  $P$  arrival, automatically detected on the vertical component of the L'Aquila earthquake strong motion records. Fig. 8 displays the time evolution of ground-motion measurements and of alert levels which would have been issued at the accelerometer sites located at an increasing epicentral distances. We note that first measurements of  $P_d$  and  $\tau_c$  are available 6–7 s after the origin time, for example, about 3 s after the first recorded  $P$  wave. An alert with level 3 is issued based on measured  $P_d$  and  $\tau_c$  at near-source stations, both parameters showing values greater than the threshold ones (0.2 cm and 0.6 s). At increasing distances (or times from the event origin) measurements of the parameter  $\tau_c$  remain stable and consistent with each other (mean value of 1.5 s), whereas  $P_d$  generally decreases, as expected, at values below the threshold one (alert level 1). Finally, the prediction error on PGV, as expressed by the log (PGVobs/PGVcal), also remain stable with time, showing a maximum variability of  $\pm 0.5$ , which is comparable to fluctuations observed for standard GMPEs (e.g. Akkar & Bommer 2010).

To illustrate the real-time operation mode of a threshold-based early warning system we have computed the snapshots of the space and time evolution of the alert levels as determined from  $P_d$  and  $\tau_c$  measurements for the L'Aquila main shock (Fig. 9). The Fig. 9 shows that the most damaged zone ( $I_{MCS} > VIII$ ) for the L'Aquila earthquake is confined within an area having a radius of about 20–30 km around the main shock epicentre.

At each time step after the first recorded  $P$  wave, the earthquake location is computed in real time by using the available  $P$  picks and the RTLloc method. At each recording site an alert level is assigned depending on the measured  $P_d$  and  $\tau_c$  values whereas the radius of the PDZ is estimated from eq. 4 using progressively updated averages of the period parameter. It is noteworthy that the first measurements of the period parameter at near-source stations provide a reliable estimation of the PDZ, which is consistent with the extent of observed largest damaged area ( $I_{MM} > VII$ ,  $I_{MCS} > VIII$ ) (Fig. 9a). As the time from the event origin progressively increases, more distant stations record the  $P$  arrival and a lower alert level is detected at stations located more than 20–30 km from the epicentre (Figs 9b and c). The spatial distribution of detected alert levels about 14 s after the origin time (10 s after the first recorded  $P$  wave) clearly defines the extent of the PDZ at almost all azimuthal sectors, except in the northeastern sector where the station coverage is poorer.

## 6 DISCUSSION AND CONCLUSIONS

We have analysed the strong motion records from modern digital accelerographs now operating in Japan, Taiwan and Italy with the aim to investigate the feasibility of a threshold-based early warning system for earthquakes in the magnitude range 4–8.

The main advantage of using strong motion records for early warning relies on the wide dynamic range of digital accelerometer

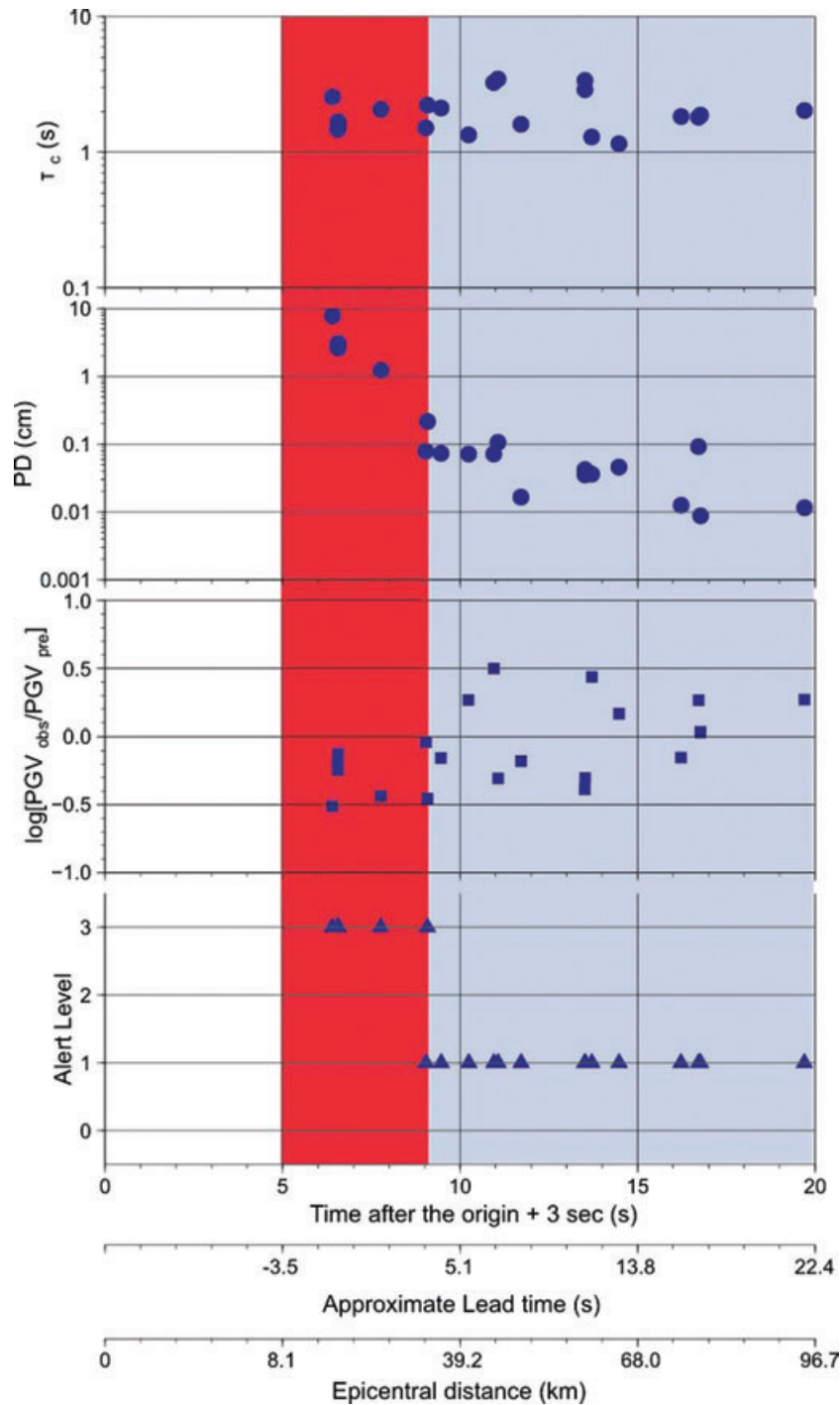


**Figure 8.** Time evolution of ground-motion measurements and the corresponding alert levels at the different stations, located at increasing distances from the epicentre of the 2009 L’Aquila main shock. From the top to the bottom, the figure shows parameters  $\tau_c$ ,  $Pd$ , the prediction error on  $PGV$  and alert level as a function of the time from the event origin. Red and light blue zones indicate the alert levels 3 and 1, respectively. Data are displayed as a function of time from the origin, lead-time and epicentral distance. The lead-time is here defined as the difference between the theoretically predicted direct  $S$ -arrival time minus the  $P$ -wave time at the near-source stations plus 3 s. The plot assumes no delay caused by telemetry/processing, which can be estimated around 1–3 s for modern computing and transmission systems.

stations, which are able to record unsaturated amplitude waveforms of moderate-to-large magnitude earthquakes even at very small epicentral distances (<10–20 km). Reducing the distance of the first recording station from the source allows to increase the lead time, for example, the time between the alert notification and the arrival time of potential destructive waves at a given target site.

The early warning method is based on the real-time measurement of two ground-motion parameters, the peak displacement  $Pd$  and the period parameter  $\tau_c$ , over a narrow time window (3 s) after the automatically detected first  $P$ -wave arrival.

$Pd$  and  $\tau_c$  are measured on the vertical component of ground motion records assuming a near vertical incidence of direct  $P$ -wave

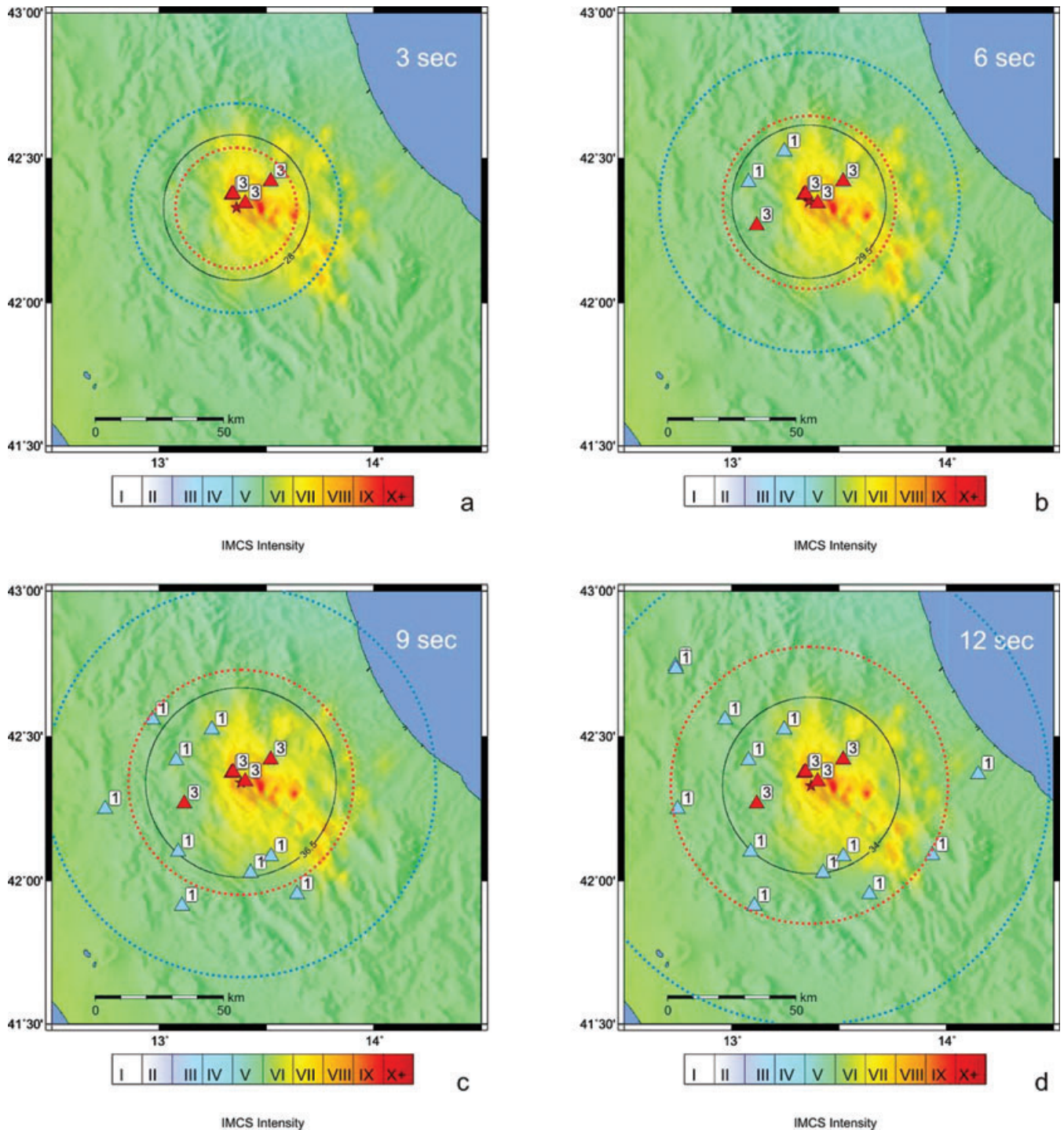


**Figure 9.** Off-line simulation of the threshold-based early warning method. The figure shows four snapshots of the space and time evolution of the recorded alert levels at 3 s, 6 s, 9 s and 12 s after the time of first  $P$  detection. The example illustrates how they can be used to define the potential damage zone (PDZ). At each time step the location is computed in real time by using the available  $P$  picks and the RTLoc method developed by Satriano *et al.* The solid black circle indicates the radius of PDZ (dimension is given in kilometres) as obtained from the updated averages of  $\tau_c$ . The dashed red and blue circles approximate the direct  $S$  and  $P$  wave front propagation away from the source epicentre. The estimation of damage has been performed by a joint group DPC and INGV which provided a detailed map of macroseismic intensity  $I_{MCS}$  (max  $I_{MCS} = IX-X$ ) (Galli *et al.* 2009), reported in figures. Note the consistency between the extents of the predicted and observed damaged zones, the latter being approximately described by  $I_{MCS} > VII-VIII$  zones of the observed macroseismic intensity distribution.

rays and near-horizontal polarized  $S$  waves. At distances smaller than about 30 km,  $S$  waves are expected to arrive within 3 s after the first  $P$ , and may have a significant amplitude on the vertical component depending on the source location and mechanism and

on the velocity model. In these cases, the application of an  $S$ -wave detector algorithm, could help in to discriminate the  $S$ -wave arrival and to better define the  $P$ -wave window for the peak measurement. However, most of up-to-date developed algorithms for  $S$ -wave

automatic picking are not well suited to operate in real time since they are based on block or batch processing of windowed data. The very basic polarization filtering used in our approach (measurements are performed along the vertical component of ground-motion records) produces reasonable results when implemented in a real-time data streaming processing chain. Only very recently, Rosenberg (2010) has proposed a promising real-time method for future applications, which is able to distinguish basic seismic phases online from a stream of three-component data with sample-to-sample resolution.

Our study confirms and generalizes the previously found empirical regression relations relating these parameters to peak ground-motion velocity and earthquake magnitude (e.g. Wu & Kanamori 2008). In particular the three determined empirical regression relations ( $\log$  PGV versus  $\log$  Pd,  $\log \tau_c$  versus  $M$  and  $\log$  Pd versus  $\log \tau_c$ ,  $\log R$ ) are consistent with all the analysed data in a wide magnitude and distance range, despite the diversity of the considered tectonic environments, earthquake faulting and regional attenuation mechanisms. In particular, we have shown that the relationship between initial  $P$ -peak displacement and final PGV can be extended up to a distance of 60 km without a significant variation of the regression parameter estimation and the standard error. These observations suggest that the empirical relationships for early warning parameters Pd and  $\tau_c$  are generally valid globally, whereas the uncertainty bounds on regression equations accounts for regional and earthquake mechanism differences.

Our proposed seismic alert methodology integrates the approach of regional and on-site early warning systems currently under development and testing worldwide. It is based on the real-time measurement of a period and peak amplitude parameter at stations located at increasing distances from the earthquake epicentre. The recorded values of early warning parameters are compared to the threshold values, which are set for a minimum magnitude  $M$  6 and  $I_{MM}$  intensity VII. These threshold values have been determined by the empirical regression analysis of strong motion data from Japan, Taiwan and Italy earthquake sequences. The main advantage of this methodology is that the potential damage effects of a moderate-to-large earthquake can be rapidly assessed and notified without estimating the earthquake location and magnitude or predicting the ground shaking level through empirical attenuation laws.

The proposed methodology provides with two estimates of the PDZ. The first one can be obtained very rapidly (well before the end of the rupture for large earthquakes) from near source stations, based upon continuously updated averages of the period parameter  $\tau_c$ . The GMPE for Pd as a function of  $\tau_c$  and hypocentral distance is used to compute the radius of PDZ, which therefore provides with a preliminary and fast but rough estimation of the PDZ, especially for large earthquake ruptures.

The proposed methodology provides with two estimates of the PDZ. The first one can be obtained very rapidly (well before the end of the rupture for large earthquakes) from near source stations, based upon continuously updated averages of the period parameter  $\tau_c$ . The GMPE for Pd as a function of  $\tau_c$  and hypocentral distance is used to compute the radius of PDZ, which therefore provides with a preliminary and fast but rough estimation of the PDZ, especially for large, finite extent, earthquake ruptures. On the other hand, as soon as new measurements of Pd and  $\tau_c$  become available from more distant stations, a more refined estimation of the potential damaged area can be inferred from the areal distribution of the maximum alert level (3 or 2). Depending on the density and spatial coverage of the accelerometric array, we expect that the shape and extent of the PDZ, as retrieved by the maximum alert level zone, better

reproduces the areal distribution and azimuthal variation of the peak ground motion around the fault rupture which is in turn related to the instrumental intensity. Within the uncertainties on parameters of the found empirical relationships for Pd and  $\tau_c$ , the method is assumed to work effectively for moderate-to-large earthquakes with an upper magnitude of 6.5, as in the case of L'Aquila earthquake. For earthquakes with a larger rupture length (and for a site at very short distance), we should probably develop another strategy, or come up with a fallback method on top of the method discussed in this paper.

Compared with the regional early warning system in which the ground-motion parameters are computed from the earthquake source parameters (location and magnitude), our approach is likely to provide more robust predictions of the potential earthquake damaging effects. However, for a more refined source parameter estimation, this methodology can be integrated with regional systems (e.g. Elarms, Allen *et al.* 2009a,b; PRESTo, Satriano *et al.* 2010) running on fast telemetered, dense strong motion networks.

At each recording site the alert level is assigned based on a decisional table with four alert levels defined upon critical values of the early warning parameter Pd and  $\tau_c$ .

Here we assume a discontinuous transition from an alert level to another, but we are working at generalizing the method through a probabilistic description of the early warning parameter distribution. The change between different alert levels is essentially controlled by the distance attenuation effect on the peak displacement parameter, whereas the real-time mapping of alert levels recorded at increasing epicentral distances allows for a preliminary but fast estimation of the areal extent of the PDZ.

Given a real-time, evolutionary estimation of earthquake location from the first  $P$  arrivals, the method furnishes an estimation of the PDZ extent as inferred from continuously updated averages of the period parameter and from the previously determined GMPE for Pd as a function of  $\tau_c$  and hypocentral distance. In our application, we have used the method for real-time earthquake location developed by Satriano *et al.* (2008) which generalizes the two-station method by Horiuchi *et al.* (2005), by jointly using the picked and not-yet detected arrival times, but giving a probabilistic estimation of the earthquake location coordinates and their uncertainties as a function of the time from the first detected  $P$  wave at the network. The method is able to provide with a first, approximate epicentral location by using just one station, applying the concept of Voronoi cells (Cua & Heaton 2007; Satriano *et al.* 2008). As far as new  $P$  picks are available, a probabilistic, evolutionary estimation of epicentre, depth and origin time is obtained, with improved accuracy. Tests on synthetic and real data, show that enough accurate and robust location estimation can be obtained using 3–4 stations depending on the station density and azimuthal coverage of the source.

The off-line application to  $M_w$  6.3, 2009 Central Italy main shock records shows the feasibility and robustness of such an approach when applied to a very densely spaced strong motion network as the one operating in Japan, Taiwan or Italy. For Italy, a special effort is now demanded to upgrade the data communication infrastructure to enable the Italian accelerometer network to process and transmit data in real time in the whole territory.

The studied case displays a very good agreement between the rapidly predicted (within a few seconds from the first recorded  $P$  wave) and observed damage zone, the latter being mapped a few days after the event from detailed macroseismic surveys. Local measurements of peak displacement and characteristic period of early  $P$  waves from near-source and distant stations allow for a faster alert notification relative to an on-site system, by increasing the

lead-time of a factor of about two depending on the epicentral distance and earthquake depth. The real-time mapping of alert levels at a set of near-source accelerometer stations can be used to predict the extent of PDZ, which is relevant information for efficient planning of the rescue operations in the immediate post-event emergency phase.

The potential use of the proposed method for early warning application within the damage zone, clearly depends on the earthquake magnitude and the extent of the damage zone itself. For the considered case of 2009 L'Aquila main shock, a moderate size earthquake, most of important damages are restricted to an area of 30–40 km around the epicentre, but earthquake strong shaking have been recorded and felt up to 100 km distance in the town of Rome. Even at short distances from the source, the true lead-time can be larger than expected from the one theoretically estimated from the first *S* arrival, since rarely the peak motion is associated to the first *S* arrival (Wu & Kanamori 2008). This is the case also for the L'Aquila event, where the time lag between the first *P* and PGV arrival is around 10–13 s for stations FMG and CLN located at epicentral distances of 20 and 30 km, respectively.

The impact of the earthquake mitigation actions triggered by an early warning system can be low (e.g. stop elevators, turn off computers, protect children under the desk), moderate (e.g. shut-off gas/electric supply, stop or slow down train) or high (e.g. shut-off large industrial plants, as nuclear, electro-thermal, chemical) depending on the intensity of the risk mitigation action and the needed time for resilience of the protected infrastructure (Iervolino *et al.* 2007). One main advantage of the proposed integrated system is the availability of a local ground-motion measurement at a distant site (as for standard on-site systems), which allows to confirm or cancel the early alert notified by *P*-wave measurements at near-source stations. Following the approach currently operated in Japan by the Japan Meteorological Agency (Allen *et al.* 2009a,b), this feature enables the end user to receive the regional warning issued by near-source stations and to incorporate it into an automated control and response system installed at the target site, specifically designed for a given early warning application.

## ACKNOWLEDGMENTS

We are grateful to the editor and reviewers Maren Böse and Holly Brown for their constructive and very helpful comments and remarks. Our work greatly benefited from discussions with Gaetano Festa, Giovanni Iannaccone and Claudio Satriano. This work has been partially funded by project INGV-DPC-S5 (2007–2009).

## REFERENCES

- Akinci, A., Malagnini, L. & Sabetta, F., 2010. Characteristics of the strong ground motions from the 6 April 2009 L'Aquila earthquake, Italy, *Soil Dyn. Earthq. Eng.*, **30**, 320–335.
- Akkar, S. & Bommer, J., 2010. Empirical equations for the prediction of PGA, PGV, and spectral accelerations in Europe, the Mediterranean region, and the Middle East, *Seism. Res. Lett.*, **81**(2), 195–206.
- Alcik, H., Ozel, O., Apaydin, N. & Erdik M., 2009. A study on warning algorithms for Instabul earthquake early warning system, *Geophys. Res. Lett.*, **36**, L00B05, doi:10.1029/2008GL036659.
- Allen, R.V., 1978. Automatic earthquake recognition and timing from single traces, *Bull. seism. Soc. Am.*, **68**, 1521–1532.
- Allen, R.M. & Kanamori, H., 2003. The potential for earthquake early warning in Southern California, *Science*, **300**(5620), 786–789.
- Allen, R.M., Brown, H., Hellweg, M., Khainovski, O., Lombard, P. & Neuhauser, D., 2009a. Real-time earthquake detection and hazard assessment by ElarmS across California, *Geophys. Res. Lett.*, **36**, L00B08, doi:10.1029/2008GL036766.
- Allen, R.M., Gasparini, P., Kamigaichi, O. & Böse, M., 2009b. The status of earthquake early warning around the world: an introductory overview, *Seism. Res. Lett.*, **80**(5), doi:10.1785/gssrl.80.5.682.
- Baer, M. & Kradolfer, U., 1987. An automatic phase picker for local and teleseismic events, *Bull. seism. Soc. Am.*, **77**, 1437–1445.
- Böse, M., Ionescu, C. & Wenzel, F., 2007. Earthquake early warning for Bucharest, Romania: novel and revised scaling relations, *Geophys. Res. Lett.*, **34**, doi:10.1029/2007GL029396.
- Böse, M., Hauksson, E., Solanki, K., Kanamori, H. & Heaton, T.H., 2009. Real-time testing of the on-site warning algorithm in southern California and its performance during the July 29, 2008 Mw 5.4 Chino Hills earthquake, *Geophys. Res. Lett.*, **36**, L00B03, doi:10.1029/2008GL036366.
- Chiarabba, C. *et al.*, 2009. The 2009 L'Aquila (central Italy) MW6.3 earthquake: main shock, *Geophys. Res. Lett.*, **36**, L18308, doi:10.1029/2009GL039627.
- Cirella, A., Piantesi, A., Cocco, M., Tinti, E., Scognamiglio, L., Michelini, A., Lomax, A. & Boschi, E., 2009. Rupture history of the 2009 L'Aquila earthquake from non-linear joint inversion of strong motion and GPS data, *Geophys. Res. Lett.*, **36**, L19304, doi:10.1029/2009GL039795.
- Cua, G. & Heaton, T., 2007. The virtual seismologist (VS) method: a Bayesian approach to earthquake early warning, in *Earthquake Early Warning Systems*, pp. 97–132, eds Gasparini, P., Manfredi, G., Zschau, J., Springer, Berlin, doi:10.1007/978-3-540-72241-0\_7.
- Espinosa-Aranda, J.M., Cuellar, A., Garcia, A., Ibarrola, G., Islas, R., Maldonado, S. & Rodriguez F.H., 2009. Evolution of the Mexican Seismic Alert System (SASMEX), *Seism. Res. Letters*, **80**(5), 694–706, doi:10.1785/gssrl.80.5.694.
- Faenza, L. & Michelini, A., 2010. Regression analysis of MCS intensity and ground motion parameters in Italy and its applications in ShakeMap, *Geophys. J. Int.*, **180**, 1138–1152.
- Faluccci, E. *et al.*, 2009. The Paganica Fault and surface coseismic ruptures caused by the 6 April 2009 earthquake (L'Aquila, central Italy), *Seismol. Res. Lett.*, **80**(6), 940–950.
- Font, Y., Kao, H., Lallemand, S., Liu, C.-S. & Chiao, L.-Y., 2004. Hypocentral determination offshore Eastern Taiwan using the Maximum Intersection method, *Geophys. J. Int.*, **158**, 655–675.
- Galli, P. *et al.*, 2009. Terremoto de L'Aquila del 6 aprile 2009: rilievo macro-sismico, distribuzione delle intensità macrosismiche ed implicazioni sistotettoniche, *Il Quaternario (Italian Journal of Quaternary Sciences)*, **22**, 235–246.
- Horiuchi, S., Negishi, H., Abe, K., Kamimura, A. & Fujinawa, Y., 2005. An automatic processing system for broadcasting system earthquake alarms, *Bull. seism. Soc. Am.*, **95**, 347–353.
- Iervolino, I., Manfredi, G. & Cosenza, E., 2007. Earthquake early warning and engineering application prospects, in *Earthquake Early Warning Systems*, p. 153, eds Gasparini, P., Manfredi, G., Zschau, J., Springer, Berlin, doi:10.1007/978-3-540-72241-0\_12.
- Kanamori, H., 2005. Real time seismology and earthquake damage mitigation, *Ann. Rev. Earth Planet Sci.*, **33**(1), 195–214.
- Maercklin, N., Zollo, A., Orefice, A., Festa, G., Emolo, A., de Matteis, R., Delouis, B. & Bobbio, A., 2010. The effectiveness of a distant accelerometer array to compute seismic source parameters: the April 2009 L'Aquila earthquake case history, *Bull. seism. Soc. Am.*, **101**(1), doi:10.1785/0120100124, in press.
- Nakamura, Y., 1984. Development of earthquake early-warning system for the Shinkansen, some recent earthquake engineering research and practical in Japan, *The Japanese National Committee of the International Association for Earthquake Engineering*, 224–238.
- Nakamura, Y., 1988. On the urgent earthquake detection and alarm system (UrEDAS), in *Proceedings 9th World Conf. Earthquake Eng.*, Vol. 7, pp. 673–678.
- Odaka, T., Ashiya, K., Tsukada, S., Sato, S., Ohtake, K. & Nozaka, D., 2003. A new method of quickly estimating epicentral distance and magnitude from a single seismic record, *Bull. seism. Soc. Am.*, **93**, 526–532.

- Pondrelli, S., Salimbeni, S., Morelli, A., Ekstrom, G., Olivieri, M. & Boschi, E., 2009. Seismic moment tensors of the April 2009, L'Aquila (Central Italy), earthquake sequence, *Geophys. J. Int.*, **180**(1), 238–242, doi:10.1111/j.1365-246X.2009.04418.x.
- Rosenberg, A., 2010. Real-time ground motion analysis: distinguishing *P* and *S* arrivals in a noisy environment, *Bull. seism. Soc. Am.*, **100**(3), 1252–1262, doi:10.1785/120090265.
- Satriano, C., Lomax, A. & Zollo, A., 2008. Real-time evolutionary earthquake location for seismic early warning, *Bull. seism. Soc. Am.*, **98**(3), doi:10.1785/0120060159.
- Satriano, C., Elia, L., Martino, C., Lancieri, M., Zollo, A. & Iannaccone, G., 2010. PRESTo, the earthquake early warning system for southern Italy: concepts, capabilities and future perspectives, *Soil Dyn. Earthq. Eng.*, doi:10.1016/j.soildyn.2010.06.008.
- Shieh, J., Wu, Y.M. & Allen, R., 2008. A comparison of  $\tau_c$  and  $\tau_{\max}^P$  form magnitude estimation in earthquake early warning, *Geophys. Res. Letters*, **35**, L20301, doi:10.1029/2008GL035611.
- Wald, D.J., Quitoriano, V., Heaton, T.H. & Kanamori, H., 1999. Relationships between peak ground acceleration, peak ground velocity and modified Mercalli intensity in California, *Earthquake Spectra*, **15**, 557–564.
- Wu, Y.M. & Teng T.L., 2002. A virtual sub-network approach to earthquake early warning, *Bull. seism. Soc. Am.*, **92**, 2008–2018.
- Wu, Y.M. & Kanamori, H., 2005. Rapid assessment of damage potential of earthquake in Taiwan from beginning of *P* waves, *Bull. seism. Soc. Am.*, **95**(3), 1181–1185, doi:10.1785/0120040193.
- Wu, Y.M. & Zhao L., 2006. Magnitude estimation using the first three seconds *P*-wave amplitude in earthquake early warning, *Geophys. Res. Letters*, **33**, L16312, doi:10.1029/2006GL026871.
- Wu, Y.M. & Kanamori, H., 2008. Development of an earthquake early warning system using real-time strong motion signals, *Sensors*, **8**, 1–9.
- Yano, T.E., Shao, G., Liu, Q., Ji, C. & Archuleta, R.J., 2009. Finite fault kinematic rupture model of the 2009 Mw 6.3 L'Aquila earthquake from inversion of strong motion, GPS and InSAR data, American Geophysical Union, Fall Meeting 2009, abstract #S34A-02.
- Zollo, A., Lancieri, M. & Nielsen, S., 2006. Earthquake magnitude estimation from peak amplitudes of very early seismic signals on strong motion, *Geophys. Res. Letters*, **33**, L23312, doi:10.1029/2006GL027795.
- Zollo, A. *et al.*, 2009a. Earthquake early warning system in southern Italy: methodologies and performance evaluation, *Geophys. Res. Letters*, **36**, L00B07, doi:10.1029/2008GL036689.
- Zollo, A. *et al.*, 2009b. The earthquake early warning system in southern Italy, in *Encyclopedia of Complexity and System Science*, **5**, 2395–2421, doi:10.1007/978-0-387-30440-3.